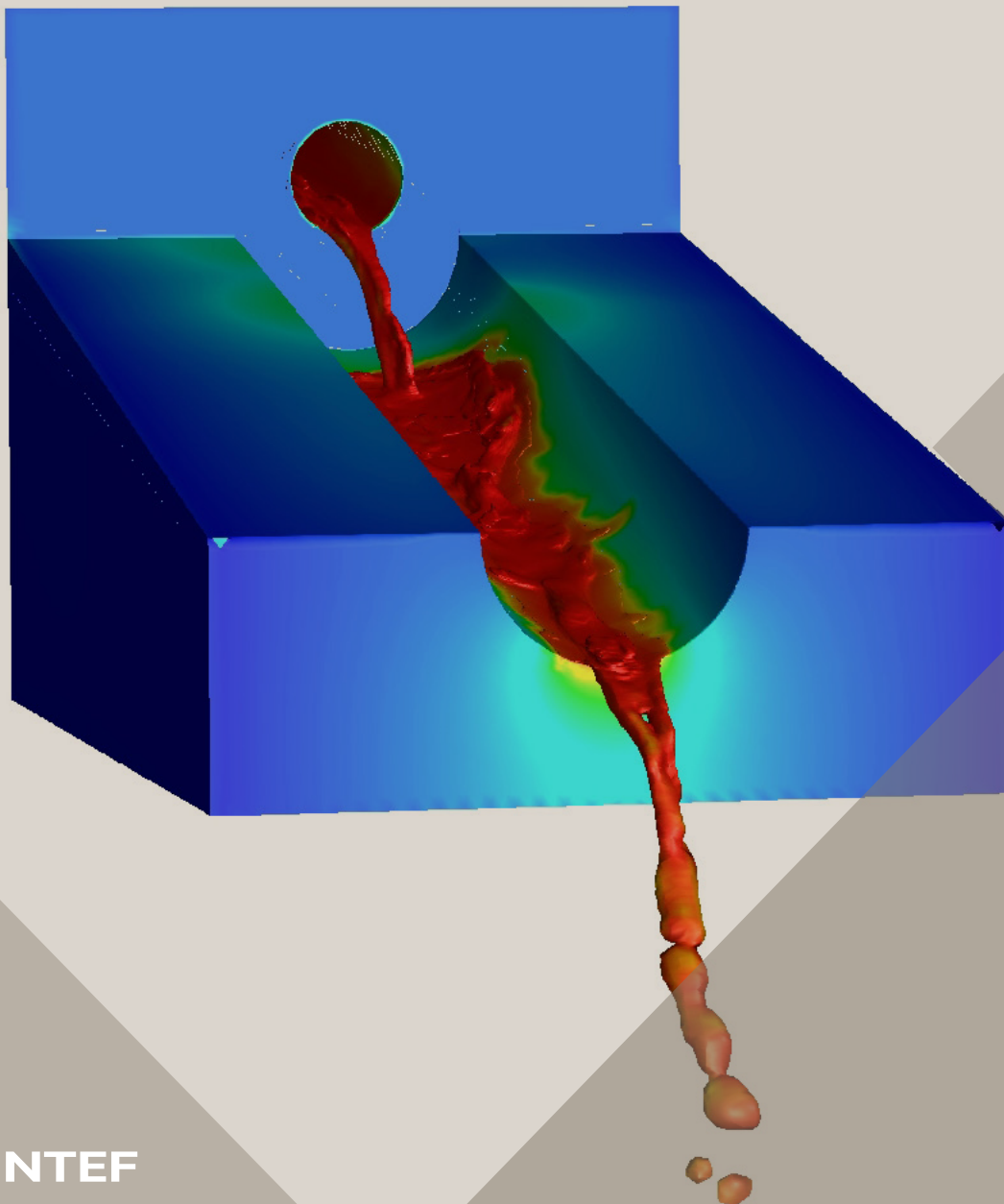14th International Conference on CFD in
Oil & Gas, Metallurgical and Process Industries
SINTEF, Trondheim, Norway, October 12–14, 2020

Proceedings from the 14th International Conference on CFD in Oil & Gas, Metallurgical and Process Industries

SINTEF

Editors:
Jan Erik Olsen, Jan Hendrik Cloete and Stein Tore Johansen

Proceedings from the 14th International Conference on CFD in Oil & Gas, Metallurgical and Process Industries

SINTEF, Trondheim, Norway
October 12–14, 2020

Numerical simulation of bubble transport and splitting dynamics for varying bifurcation angle

Mahesh S. Nagargoje[1]*, Raghvendra Gupta[1]‡

[1] IIT Guwahati, 781039 Guwahati, India

* E-mail: nmahesh@iitg.ac.in
‡ E-mail: guptar@iitg.ac.in

ABSTRACT

Gas embolotherapy is a recent potential cancer treatment. The technique is based on starving the tumors by cutting off the blood supply using perfluorocarbon (PFC) bubbles. The volatile PFC droplets are injected in the circulatory system, and in the region of the tumor, these droplets are made to vaporize using high-intensity ultrasound pulses. As the bubbles are expected to encounter bifurcation during its flow in the vessels, it is imperative to develop an understanding of bubble splitting at the bifurcations to avoid nonhomogeneous splitting, undesirable bioeffects. Splitting dynamics has been studied for symmetric bifurcation angle.

In this work, we investigate the splitting dynamics of a gas bubble at the symmetric, two-dimensional (2D) bifurcation. The volume of fluid method, which employs a single fluid formalism to solve for two-phase flow by considering an additional advection equation for a color function to identify the phases, is used to model the flow. The pressure jump caused by surface tension is modeled by approximating the surface tension force as a body force in the vicinity of the interface. Initially, the entire domain is filled with the liquid phase, i.e., blood. As the flow Reynolds number is 10-100, blood is considered to be a Newtonian fluid. Once a steady solution for liquid-only flow is obtained, a bubble is introduced in the channel having a capsular shape. The bubble takes a steady shape after a few ms.

The results show that at the higher capillary number (Ca = 0.0231), homogenous splitting occurs for all bifurcation angles. Similarly, at lower capillary number (Ca = 0.00231) and low bifurcation angle ($\alpha = \beta = 15°$, 30°, and 45°), bubble split homogenously. In contrast, at a higher bifurcation angle ($\alpha = \beta = 60°$) bubble does not split and is pushed in the daughter vessel. The critical bifurcation angle exists between $\alpha = \beta = 45°$-60°, where capillary forces become dominant and the bubble does not split.

Keywords: CFD, multiphase flow, gas embolotherapy.

NOMENCLATURE

Greek Symbols
ρ Mass density, [kg/m^3].
μ Dynamic viscosity, [kg/m.s].
σ Surface tension force, [N/m]
τ Shear stress tensor, [N/m^2]

Latin Symbols
p Pressure, [Pa].
u Velocity, [m/s].
κ Curvature, [m^{-1}]

INTRODUCTION

Gas embolotherapy is a potential cancer treatment, in which intra-arterial blood supply to cancer tumor is cut off using gas bubbles (Bull, 2007). In this treatment, the perfluorocarbon (PFC) microdroplets (~6 μm in diameter) are passed through the arteries and selectively vaporized at the desired tumor location using high-intensity ultrasound (Kripfgans, O. D., Fowlkes, J. B., Miller, D. L., Eldevik, O. P., & Carson, 2000; Kripfgans et al., 2005; Qamar et al., 2010). Due to ultrasound, these droplets get vaporized, and the bubble formation (~150 times volume expansion) takes place to occlude the blood flow covering an entire cross-section of the blood vessel (Kang, S. T., Huang, Y. L., & Yeh, 2014; Kang et al., 2014; Kripfgans et al., 2004). For effective treatment, a large number of these bubbles should pass through tumor affected vessels. The generated bubbles travel into smaller capillaries and eventually occlude the capillaries with a sausage-shaped configuration (Samuel, S., Duprey, A., Fabiilli, M. L., Bull, J. L., & Brian Fowlkes, 2012). The capillaries are more likely to damage because of its fragile structure, thin vessel wall, and lower blood velocity. Due to acoustic droplet vaporization (ADV) occurred in the capillaries, the expansion of droplets takes place with a higher wall velocity in the order of hundreds of meters per second (Kripfgans et al., 2004; Qamar et al., 2010; Wong et al., 2011). The bubble dynamics in capillaries lead to undesired bioeffects, such as endothelial damage and rupture of the capillaries (Bull, 2005; Wong and Bull, 2011). This work of Embolotherapy has started with experiments of bubble transport in bifurcation models to predict the bubble lodging and occlusion of vessels (Calderón et al., 2006, 2005; Eshpuniyani et al., 2005).

In the past decade, the number of researchers has been explained the various parameters in the gas embolotherapy process. Recently, it has been adopted for the model of hepatocellular carcinoma in mice, which proved that tumor growth had been halted using a gas embolotherapy technique (Harmon et al., 2019). The

multiphase flow at bifurcation and control of ADV remains an active topic of research for experimental (Fabiilli et al., 2009; Lo et al., 2007; Wong et al., 2011) and numerical work (Poornima and Vengadesan, 2012; Qamar et al., 2017; Ye and Bull, 2006, 2004), which analyzes the splitting behavior and lodging of bubbles in the capillaries. The present study focuses on bubble behavior at bifurcation after vaporization and before lodging in smaller vessels. For a successful treatment, at least 78% of blood supply to the tumor needs to be occluded (Di Segni, R., Young, A. T., Qian, Z., & Castaneda-Zuniga, 1997). Various factors, such as blood flow rate, gravity, bubble size, and vessel geometry, affect the splitting behavior of the bubble at the bifurcation. Different regimes and splitting behavior were observed at bifurcations. Faster flow rates and weaker gravitational effects result in even splitting in daughter vessels, whereas at lower flow rates, the splitting is uneven, depends on roll angle/gravity, the angle made by horizontal plane with mother vessel axis (Eshpuniyani et al., 2005). Numerical simulations observed homogenous, non-homogenous splitting, and no splitting. For constant inlet droplet size, droplet splits at the higher capillary number, and no splitting observed at the lower capillary number (Carlson et al., 2010). Similar behavior was observed for bubble splitting. With the decrease in capillary number, non-homogenous splitting behavior increases, and at below critical value of a capillary number, the bubble does not split (Calderón et al., 2005). At higher Reynolds number (low capillary numbers) bubble does not split, while at low Reynolds number (higher capillary numbers) bubble splits at bifurcation into two daughter tubes (Qamar et al., 2017). For symmetric bifurcations, the splitting ratio is one, while asymmetric bifurcation ratios show a splitting ratio of less than one (Poornima and Vengadesan, 2012). Boundary element computations of bubble splitting found that bubble splitting ratio increases with increasing bubble driving pressure while it decreases with increasing bifurcation angle (Calderon et al., 2010).

Most of the studies available in the literature were focused on the splitting of the bubble in a fixed bifurcation angle. At the same time, human vascular arterial networks do not have a symmetric angle everywhere. Our previous work studied the flow behavior of single-phase flow in various bifurcation angle combinations (Nagargoje and Gupta, 2020). Successful treatment needs to understand the bubble splitting behavior in the bifurcation to occlude the tumorous vessel. This work addresses this gap by investigating the steady blood flow and PFC bubble in two-dimensional, symmetric bifurcating networks using commercial computational fluid dynamics (CFD) package ANSYS Fluent 19.2 for symmetric bifurcation angles varying in the range 30°-120°. A recent study shows that the splitting ratio does not change for pulsating and constant flows (Valassis et al., 2012). So we have considered the inlet flow to be steady for all simulations.
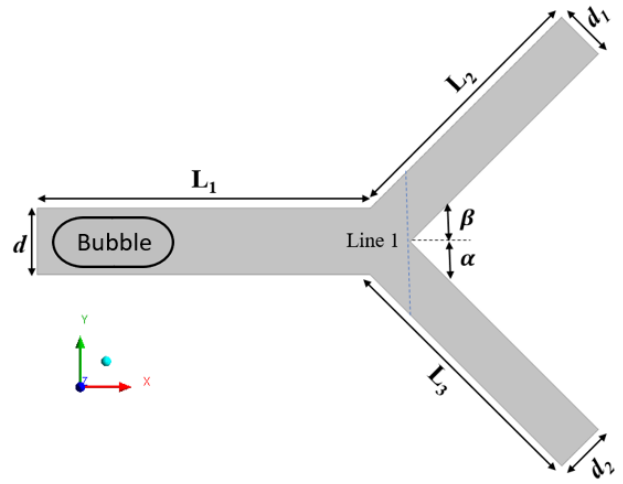

Fig. 1 Schematic of the bifurcation geometry where: $d = 1$ mm; d_1, $d_2 = 0.78$ mm; L_1, L_2, $L_3 = 5d$; α, β are angle made by daughter vessels in-plane with mother vessel.

METHODOLOGY

A two dimensional arterial model with mother vessel (d) and two daughter vessels (d_1 and d_2), as shown in Fig. 1, is used for modeling the bubble splitting in the present study. The diameter of the mother vessel is 1mm, and that of daughter vessels is 0.78 mm each. The values of the bifurcation angles (α, β) are varied symmetrically ($\alpha = \beta$) from 30°-120°. Blood (Newtonian) is modeled as a primary phase (liquid) with a viscosity of 0.0035 Pa. s and a density of 1060 kg/m^3. The secondary phase (gas) is a perfluorocarbon (PFC) gas with a viscosity of 2×10^{-5} Pa. s and a density of 12 kg/m^3 (Poornima and Vengadesan, 2012).

Numerical modeling

The transport of the PFC bubble through a blood-filled arterial bifurcation model is a multiphase (gas-liquid) problem. Blood is modeled as a Newtonian fluid. We have used a commercial CFD code finite volume based ANSYS Fluent 19.2 and inbuilt continuum surface force (CSF) based volume of fluid (VOF) method to track the gas-liquid interface, in which a single set of momentum equations is solved. VOF approach is used widely due to its high accuracy, flexibility, and excellent stability.

The governing equations of the VOF formulation are as follows:

Equation of Continuity
$$\nabla.\boldsymbol{u} = 0 \tag{1}$$
Equation of momentum conservation:
$$\rho\left(\frac{\partial \boldsymbol{u}}{\partial t} + (\boldsymbol{u}.\nabla)\boldsymbol{u}\right) = -\nabla P + \nabla.\boldsymbol{\tau} + \boldsymbol{F} \tag{2}$$
$$\boldsymbol{\tau} = \mu(\nabla\boldsymbol{u} + \nabla\boldsymbol{u}^T) \tag{3}$$
Volume fraction equation:
$$\frac{\partial \alpha_G}{\partial t} + \boldsymbol{u}.\nabla\alpha_G = 0, \tag{4}$$
At the interfacial cells, the mixture density, and viscosity have been evaluated as the average values of the two phases weighted by their volume fraction,
$$\rho = \alpha_L\rho_L + \alpha_G\rho_G \tag{5}$$
$$\mu = \alpha_L\mu_L + \alpha_G\mu_G \tag{6}$$
The body force term "F" on RHS of equation of eq. (2) includes the surface tension force (σ), which has been modeled by the continuum surface force (CSF) proposed

by Brackbill et al.(Brackbill et al., 1992) and it can be written as follow,

$$\boldsymbol{F} = \sigma \kappa \boldsymbol{n} \tag{7}$$

Where κ is the curvature and can be written by following equation:

$$\kappa = \nabla . \hat{\boldsymbol{n}} \tag{8}$$

Where, η is the normal vector given by

$$\boldsymbol{n} = \nabla \alpha \tag{9}$$

And unit normal vector(n) is given by

$$\hat{\boldsymbol{n}} = \frac{\boldsymbol{n}}{|\boldsymbol{n}|} \tag{10}$$

The arterial model is meshed using ANSYS meshing. After the mesh independence study, the model is imported to ANSYS Fluent for further simulations. Blood is considered as the primary phase (liquid) and PFC bubble (gas) as the secondary phase in VOF formulation. The bubble is patched initially 1 mm away from the inlet having length 1.5 times mother vessel diameter. The different Reynolds number, based on mother tube diameter, is used as 10, 100. Surface tension between the PFC bubble and blood is taken as 0.05 N/m. For the unsteady-state simulations, a fully developed parabolic velocity profile with constant velocity is used at the inlet. At the outlet pressure, the outlet boundary condition is imposed with gauge pressure equal to zero. The PISO scheme is used for the pressure velocity coupling. The body force weighted scheme is used for pressure interpolation, and the quadratic upwind interpolation for convection kinetics (QUICK) scheme is used to discretize the terms in the momentum equations. For interpolating the interface between fluids, the modified HRIC scheme is used to get a sharp interface. The first-order implicit time marching scheme with non-iterative time advancement is used for discretization of the unsteady term. The simulations are advanced with a time increment of 1×10^{-7} s.

RESULTS

Figure 2 shows the pressure distribution and bubble shape variation at various time instances during the splitting process. Initially, the pressure at the inner wall of bifurcation is high while low near to the outer wall. The pressure value in the mother tube suddenly increases as the bubble reaches the bifurcation. The bubble occupies entire cross-section of vessel and creates obstruction to fluid flow through the small film thickness around the bubble after reaching at bifurcation.

The effect of the symmetric bifurcation angle on the dynamics of the bubble neck during the final stage of the breaking of the bubble is shown in Fig. 3. Throughout the rupture process, the shape of the bubble head does not change due to the presence of a gap between the bubble and channel wall. However, the bubble neck width changes continuously and is highly deformed. It can be seen as time passes, the neck width gradually decreases to zero at the bifurcation, and then the bubble is pinched-off. The bubble neck is flat for lower bifurcation angle i. e. $\alpha = \beta = 15°$, but as the bifurcation angle increases, the neck of the bubble becomes more concave. For a higher bifurcation angle, there is more possibility of retaining small satellites of the PFC bubble due to the presence of a thin tail between the neck of the bubble and the wall of bifurcation. These small satellites may contribute to unexpected bio-effects such as endothelial suffocation or

acoustic cavitation. These satellites may affect the splitting behavior of the next train of bubbles.

Figure 4, and 5 shows the splitting behavior of the PFC bubble at the bifurcation point for $\alpha = \beta = 15°$, and $45°$ at Re = 10, respectively. Initially, the bubble is close to the wall, separated by a thin film (δ) using Bretherton's correlation(Bretherton, 1961). The shape of the bubble starts to change at bifurcation due to resistance to flow around the bubble, and the concave shape of the bubble takes place at trailing end. After the bubble neck reaches a bifurcation, the thin film stretches, and the bubble splits into two equal-size daughter bubbles in a homogenous way, as shown in Fig. 4, and 5 (t_3). The x-component of velocity at the bifurcation point is parabolic along line 1 at time instance t_1 and t_3, as shown in Fig. 4, 5(a). The maximum velocity is skewed towards the inner wall of bifurcation. The volume of the fluid method was used, which shown the velocities of gas and liquid depending on its position. During the pinch-off stage of bubble break up (t_2), the velocity profiles along line 1 are symmetric along both sides of daughter vessel, and the deviations of velocity are very small from steady-state (t_1 and t_3). Due to symmetry in the velocity profile during pinch-off, the bubble splits in a homogenous fashion. The symmetry in the velocity profile is observed for the y-velocity component as well, as shown in Fig. 4, 5(b). Once the bubble passed into the daughter vessels, flow regains the steady-state at line 1, as shown in Fig. 4, 5(a, b) (t_1 and t_3).
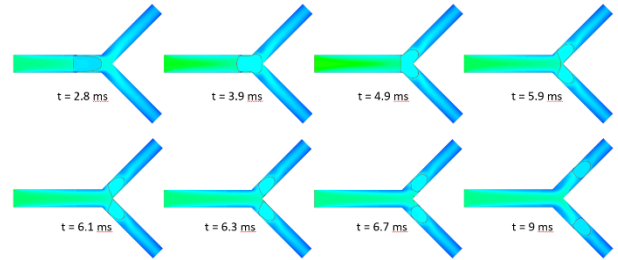

Fig. 2 Pressure contours and bubble shape at various time instance for $\alpha = \beta = 45°$ (Re = 100 and Ca = 0.0231).
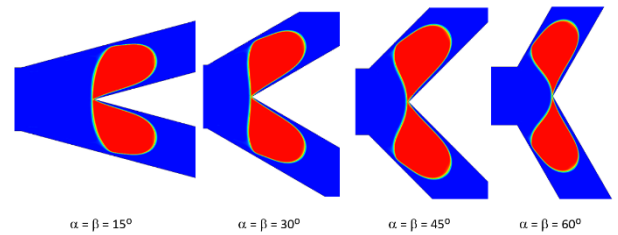

Fig. 3 Splitting behavior of PFC bubble at the bifurcation point for varying symmetric bifurcation angle at Ca = 0.0231.

For the larger bifurcation angle ($\alpha = \beta = 60°$), the bubble does not split and goes into the lower daughter vessel, as shown in Fig. 6 (t_3). The bubble enters the bifurcation in the usual manner as explained earlier, but the portion in the lower channel remains close to the vessel wall, while the portion in the upper channel separates and swings downward. This phenomenon of bubble behavior is called no splitting behavior. At lower Capillary number, the surface tension dominates over the inertial force, and the bubble reverses back into the lower vessel and completely pass through it. A similar kind of reversal splitting was observed for liquid droplets (Calderon et al., 2010; Carlson et al., 2010). Due to

stronger capillary force, a larger curvature is observed at the bubble neck, resulting in a larger radius of the gas-liquid interface. As the perturbation grows, the bubble migrates into the lower daughter vessel. The stronger recirculation's observed in the upper daughter vessel, which increases the pressure difference between the upper and lower daughter vessel. The velocity profiles at the bifurcation point along line 1 reveal much about the reversal splitting. The bubble remains stable before reaching to the bifurcation. Once it reaches the bifurcation, the x-component of velocity shows a very high speed and high-velocity gradient between two daughter vessels at the pinch-off stage, as shown in Fig. 6(a). The same phenomena are observed for the y-velocity component and can be seen in Fig. 6(b). From the discussion of bubble splitting in symmetric bifurcation, it was observed that the homogenous splitting of the bubble is observed for higher Reynolds numbers at all bifurcation angles. Whereas no splitting is observed at low Reynolds number (Re = 10) and high bifurcation angle ($\alpha = \beta = 60°$). For higher bifurcation angle ($\alpha = \beta = 60°$) and small Reynolds number (Re = 10), we found the bubble does not split and passes into the lower daughter vessel.
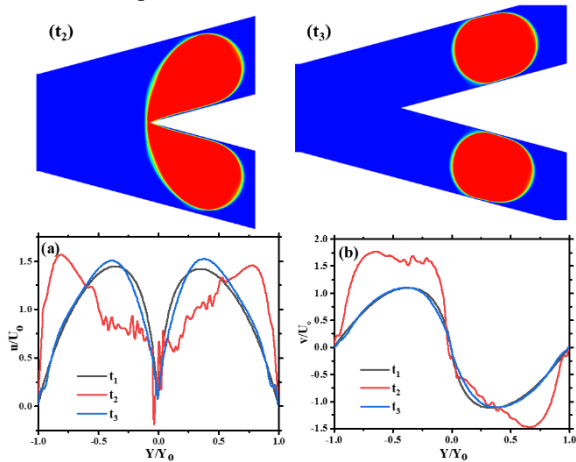

Fig. 4 Splitting behavior of PFC bubble at the bifurcation point for $\alpha = \beta = 15°$ (Re = 10 and Ca = 0.00231)) at different time instance, top: bubble volume fraction (Red colour), bottom: (a) x-velocity and (b) y-velocity profiles along line 1.

Fig. 5 Splitting behavior of PFC bubble at the bifurcation point for $\alpha = \beta = 45°$ (Re = 10 and Ca = 0.00231 at different time instance, top: bubble volume fraction (Red colour), bottom: (a) x-velocity and (b) y-velocity profiles along line 1.

Fig. 6 Splitting behavior of PFC bubble at the bifurcation point for $\alpha = \beta = 60°$ (Re = 10 and Ca = 0.00231 at different time instance, top: bubble volume fraction (Red colour), bottom: (a) x-velocity and (b) y-velocity profiles along line 1.
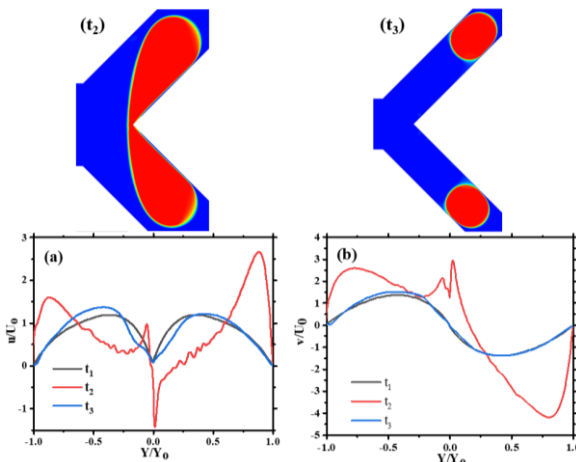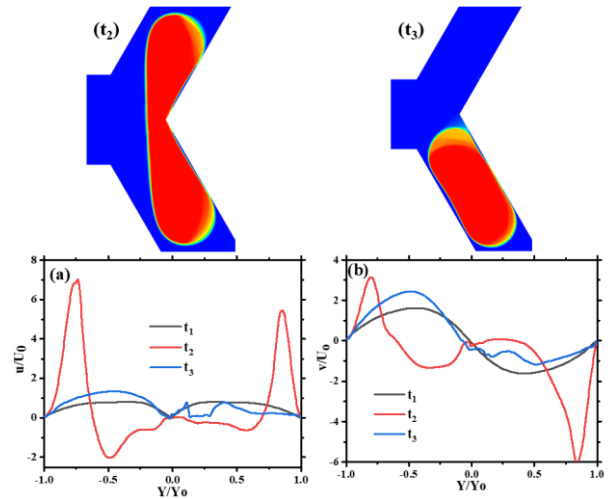
STUDY LIMITATIONS

The present study's major limitation is the assumption of blood as a Newtonian fluid and two-dimensional arterial geometry. The blood should be modeled as a non-Newtonian fluid in the capillaries. The bubble shape may vary in three-dimensional vessel geometry due to the presence of secondary flow. Future studies should include the influence of asymmetry in bifurcation angle, multiple droplet splitting effect, and bubble splitting in three-dimensional bifurcating vessels for non-Newtonian blood flow.

CONCLUSIONS

The present paper reports on two-dimensional numerical simulations of droplet dynamics in a bifurcating channel for varying bifurcation angles symmetrically. The splitting and non-splitting flow regimes have been observed. We showed the effect of the capillary number on the bifurcation angle.

The PFC bubble split homogenously at a higher value of the capillary number (Ca = 0.0231), where viscous force dominates over the surface tension force, and the bubble splits equally. Similarly, in the lower bifurcation angle ($\alpha = \beta < 60$) and at the lower capillary number (Ca = 0.00231) observed a splitting behavior. But, for a higher bifurcation angle ($\alpha = \beta = 60$), and lower capillary number (Ca = 0.00231) bubble does not split and goes into a lower daughter vessel. In non-splitting behavior, surface tension force dominates over viscous force.

REFERENCES

ANSYS Academic Research Fluent, Release 19.2, Help System, Theory Guide, ANSYS, Inc., 2019.

Brackbill, J.U., Kothe, D.B., Zemach, C., 1992. A continuum method for modeling surface tension. J. Comput. Phys. 100, 335–354.

Bretherton, F.P., 1961. The motion of long bubbles in tubes. J. Fluid Mech. 10, 166–188.

Bull, J.L., 2007. The application of microbubbles for targeted drug delivery. Expert Opin. Drug Deliv. 4, 475–493.

Bull, J.L., 2005. Cardiovascular bubble dynamics. Crit. Rev. Biomed. Eng. 33, 299–346.

Calderon, A.J., Eshpuniyani, B., Fowlkes, J.B., Bull, J.L., 2010. A boundary element model of the transport of a semi-infinite bubble through a microvessel bifurcation. Phys. Fluids 22, 1–11.

Calderón, A.J., Fowlkes, J.B., Bull, J.L., 2005. Bubble splitting in bifurcating tubes: A model study of cardiovascular gas emboli transport. J. Appl. Physiol. 99, 479–487.

Calderón, A.J., Heo, Y.S., Huh, D., Futai, N., Takayama, S., Fowlkes, J.B., Bull, J.L., 2006. Microfluidic model of bubble lodging in microvessel bifurcations. Appl. Phys. Lett. 89, 2004–2007.

Carlson, A., Do-Quang, M., Amberg, G., 2010. Droplet dynamics in a bifurcating channel. Int. J. Multiph. Flow 36, 397–405.

Di Segni, R., Young, A. T., Qian, Z., & Castaneda-Zuniga, W.R., 1997. Embolotherapy: agents, equipment, and techniques. Interv. Radiol. 3.

Eshpuniyani, B., Fowlkes, J.B., Bull, J.L., 2005. A bench top experimental model of bubble transport in multiple arteriole bifurcations. Int. J. Heat Fluid Flow 26, 865–872.

Fabiilli, M.L., Haworth, K.J., Fakhri, N.H., Kripfgans, O.D., Carson, P.L., Fowlkes, J.B., 2009. The role of inertial cavitation in acoustic droplet vaporization. IEEE Trans. Ultrason. Ferroelectr. Freq. Control 56, 1006–1017.

Harmon, J.S., Kabinejadian, F., Seda, R., Fabiilli, M.L., Kuruvilla, S., Kuo, C.C., Greve, J.M., Fowlkes, J.B., Bull, J.L., 2019. Minimally invasive gas embolization using acoustic droplet vaporization in a rodent model of hepatocellular carcinoma. Sci. Rep. 9, 1–11.

Kang, S. T., Huang, Y. L., & Yeh, C.K., 2014. Characterization of acoustic droplet vaporization for control of bubble generation under flow conditions.

Kang, S.T., Lin, Y.C., Yeh, C.K., 2014. Mechanical bioeffects of acoustic droplet vaporization in vessel-mimicking phantoms. Ultrason. Sonochem. 21, 1866–1874.

Kripfgans, O. D., Fowlkes, J. B., Miller, D. L., Eldevik, O. P., & Carson, P.L., 2000. Acoustic droplet vaporization for therapeutic and diagnostic applications. Ultrasound Med. Biol. 26, 1177–1189.

Kripfgans, O.D., Fabiilli, M.L., Carson, P.L., Fowlkes, J.B., 2004. On the acoustic vaporization of micrometer-sized droplets. J. Acoust. Soc. Am.

116, 272–281.

Kripfgans, O.D., Orifici, C.M., Carson, P.L., Ives, K.A., Eldevik, O.P., Fowlkes, J.B., 2005. Acoustic droplet vaporization for temporal and spatial control of tissue occlusion: A kidney study. IEEE Trans. Ultrason. Ferroelectr. Freq. Control 52, 1101–1108.

Lo, A.H., Kripfgans, O.D., Carson, P.L., Rothman, E.D., Fowlkes, J.B., 2007. Acoustic droplet vaporization threshold: Effects of pulse duration and contrast agent. IEEE Trans. Ultrason. Ferroelectr. Freq. Control 54, 933–945.

Nagargoje, M., Gupta, R., 2020. Effect of asymmetry on the flow behavior in an idealized arterial bifurcation. Comput. Methods Biomech. Biomed. Engin. 23, 232–247.

Poornima, J., Vengadesan, S., 2012. Numerical simulation of bubble transport in a bifurcating microchannel: A preliminary study. J. Biomech. Eng. 134, 1–10.

Qamar, A., Warnez, M., Valassis, D.T., Guetzko, M.E., Bull, J.L., 2017. Small-bubble transport and splitting dynamics in a symmetric bifurcation. Comput. Methods Biomech. Biomed. Engin. 20, 1182–1194.

Qamar, A., Wong, Z.Z., Fowlkes, J.B., Bull, J.L., 2010. Dynamics of acoustic droplet vaporization in gas embolotherapy. Appl. Phys. Lett. 96, 1–4. https://doi.org/10.1063/1.3376763

Samuel, S., Duprey, A., Fabiilli, M. L., Bull, J. L., & Brian Fowlkes, J., 2012. In vivo microscopy of targeted vessel occlusion employing acoustic droplet vaporization. Microcirculation 19, 501–509.

Valassis, D.T., Dodde, R.E., Esphuniyani, B., Fowlkes, J.B., Bull, J.L., 2012. Microbubble transport through a bifurcating vessel network with pulsatile flow. Biomed. Microdevices 14, 131–143.

Wong, Z.Z., Bull, J.L., 2011. Vascular bubbles and droplets for drug delivery. J. Drug Deliv. Sci. Technol. 21, 355–367.

Wong, Z.Z., Kripfgans, O.D., Qamar, A., Fowlkes, J.B., Bull, J.L., 2011. Bubble evolution in acoustic droplet vaporization at physiological temperature via ultra-high speed imaging. Soft Matter 7, 4009–4016.

Ye, T., Bull, J.L., 2006. Microbubble expansion in a flexible tube. J. Biomech. Eng. 128, 554–563.

Ye, T., Bull, J.L., 2004. Direct numerical simulations of micro-bubble expansion in gas embolotherapy. J. Biomech. Eng. 126, 745–759.